iScience, Volume *27*

Supplemental information

Genome-scale CRISPR-Cas9 screen identifies host factors as potential therapeutic targets for SARS-CoV-2 infection

Madoka Sakai, Yoshie Masuda, Yusuke Tarumoto, Naoyuki Aihara, Yugo Tsunoda, Michiko Iwata, Yumiko Kamiya, Ryo Komorizono, Takeshi Noda, Kosuke Yusa, Keizo Tomonaga, and Akiko Makino

Table S4. sgRNA sequences for CRISPR–Cas9 screening. Related to Figure 1

Gene	sgRNA_ID	sgRNA sequence
DAXX	DAXX_v3_6-3	CCGGCGCCTTCGGGAAAAC
DAXX	DAXX_v3_6-4	CCGACTCATGGCCAAACTC
TRIM33	TRIM33_v3_6-2	ATGCTTCACCTGCCGGGAA
TRIM33	TRIM33_v3_6-4	TTGCAGAGCCGGCGTGAGG
EHMT1	EHMT1_v3_6-4	ACTCGGATAGCGGAAAATG
EHMT1	EHMT1_v3_6-6	CGCCGACGTCAAGGTCCAC
EHMT2	EHMT2_v3_6-2	AAGAGGTGACCATCCCCCG
EHMT2	EHMT2_v3_6-4	GATTGACCGCATCAGCGAG
MED12	MED12_v3_6-1	TTGCGATGTCATTCACCCT
MED12	MED12_v3_6-3	GTACTGCACGTGTCGTGGC
MED23	MED23_v3_6-1	CCAGGAGGTTCATAGGTAA
MED23	MED23_v3_6-2	ACAGCATTAGGTAGCTCAG
VPS29	VPS29_v3_7-1	CTCTGCAACAGGGCTAAGC
VPS29	VPS29_v3_7-6	ACTATCTCAAGACTCTGGC
VPS35	VPS35_v3_6-5	CGAAGAAACAGACCCCTCA
VPS35	VPS35_v3_6-6	CAAGGGATGTTGCACACCA
NF2	NF2_v3_9-1	ACAGTGGCCTGGCTCAAAA
NF2	NF2_v3_9-7	CCGGCACACCAAATCAAAG
TRIM28	TRIM28_v3_6-2	TGGTTCGCATCCTGGGCGT
TRIM28	TRIM28_v3_6-3	TACAGGCCGAGTGCAAACA

Table S5. Primer sequences for RT-qPCR. Related to Figure 2, 3, and 6

Gene	species	Fw/Rv	Primer sequence	Reference
ACE2	homo sapiens	Fw	TGCAGACCAAAGCATCAAAG	20
		Rv	AATTAGCCACTCGCACATCC	
CXCL10	homo sapiens	Fw	GTGGCATTCAAGGAGTACCTC	53
		Rv	GCCTTCGATTCTGGATTCAGACA	
GAPDH	homo sapiens	Fw	ATTTGGCTACAGCAACAGGGT	54
		Rv	AACTGTGAGGGGAGATTCAGTG	
IFNB1	homo sapiens	Fw	AAACTCATGAGCAGTCTGCA	55
		Rv	AGGAGATCTTCAGTTTCGGAGG	
IL-6	homo sapiens	Fw	CCTGAACCTTCCAAAGATGGC	56
		Rv	TTCACCAGGCAAGTCTCCTCA	
TNFα	homo sapiens	Fw	ATGAGCACTGAAAGCATGATCC	53
		Rv	GAGGGCTGATTAGAGAGAGGTC	
ACE2	Mesocricetus auratus	Fw	GAAGAGGCTGTCAGGTTGTC	57
		Rv	TGCCAACCACTACAATTCCC	
IL-6	Mesocricetus auratus	Fw	CCTGGCTGTATGGACAATGACT	
		Rv	AGTCCAGAAGACCAGAGGTGA	
RPL18	Mesocricetus auratus	Fw	GTTTATGAGTCGCACTAACCG	58
		Rv	TGTTCTCTCGGCCAGGAA	
TMPRSS2	Mesocricetus auratus	Fw	ATGGAGTGCATGTCTTCAGGC	
		Rv	GGAGCTGTGATCAGTGTGGTG	
TNFα	Mesocricetus auratus	Fw	CTGAACTTCGGGGTGATCGG	59
		Rv	TGAGAGACATGCCGTTGGC	

Supplementary Figures

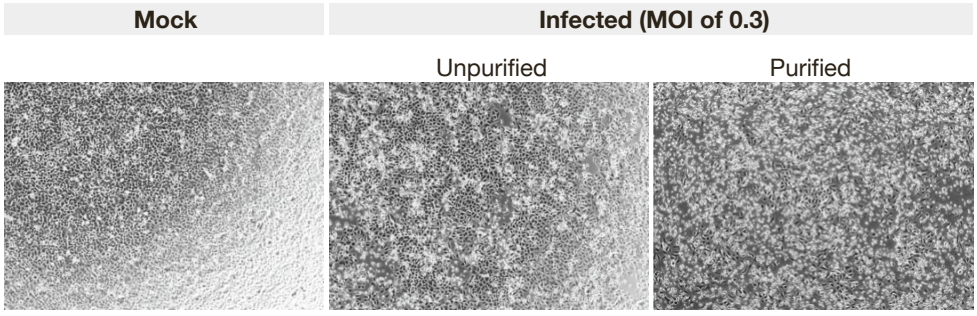

Fig. S1. Cytopathic effects induced by infection with purified and unpurified SARS-CoV-2. Related to Figure 1

Representative microscopic images of A549-hACE2 cells infected with SARS-CoV-2 that was either unpurified or purified via ultracentrifugation. Images were captured 3 days post-infection to illustrate the cytopathic effects in the cells.

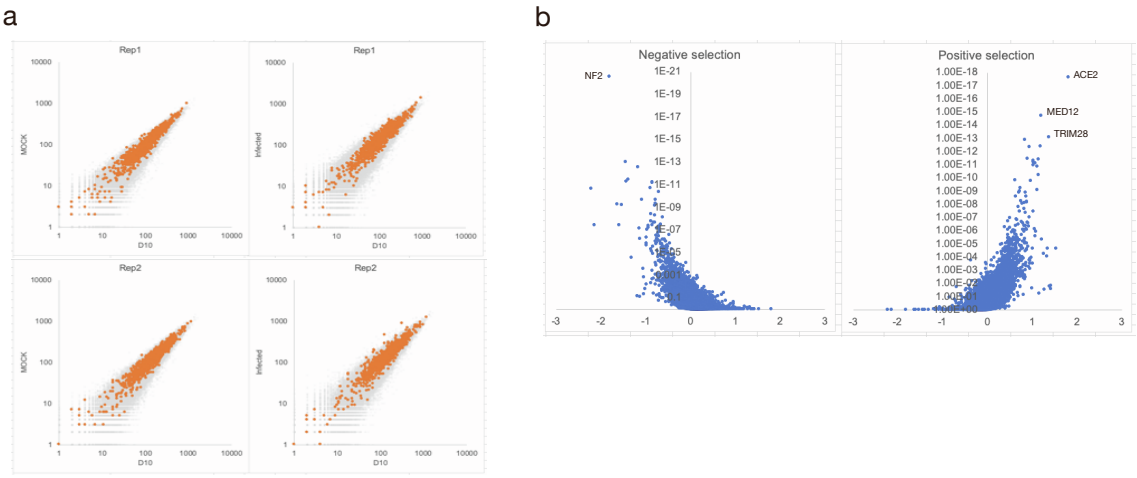

Fig. S2. CRISPR–Cas9 screening data analysis. Related to Figure 1

(a) Scatterplot of gRNA counts in gCTRL (n=1004, highlighted in orange) cells to confirm the quality of screening. Comparison between preinfection versus mock and preinfection versus infected. (b) Volcano plot of gRNA change compared between mock and infected cells.

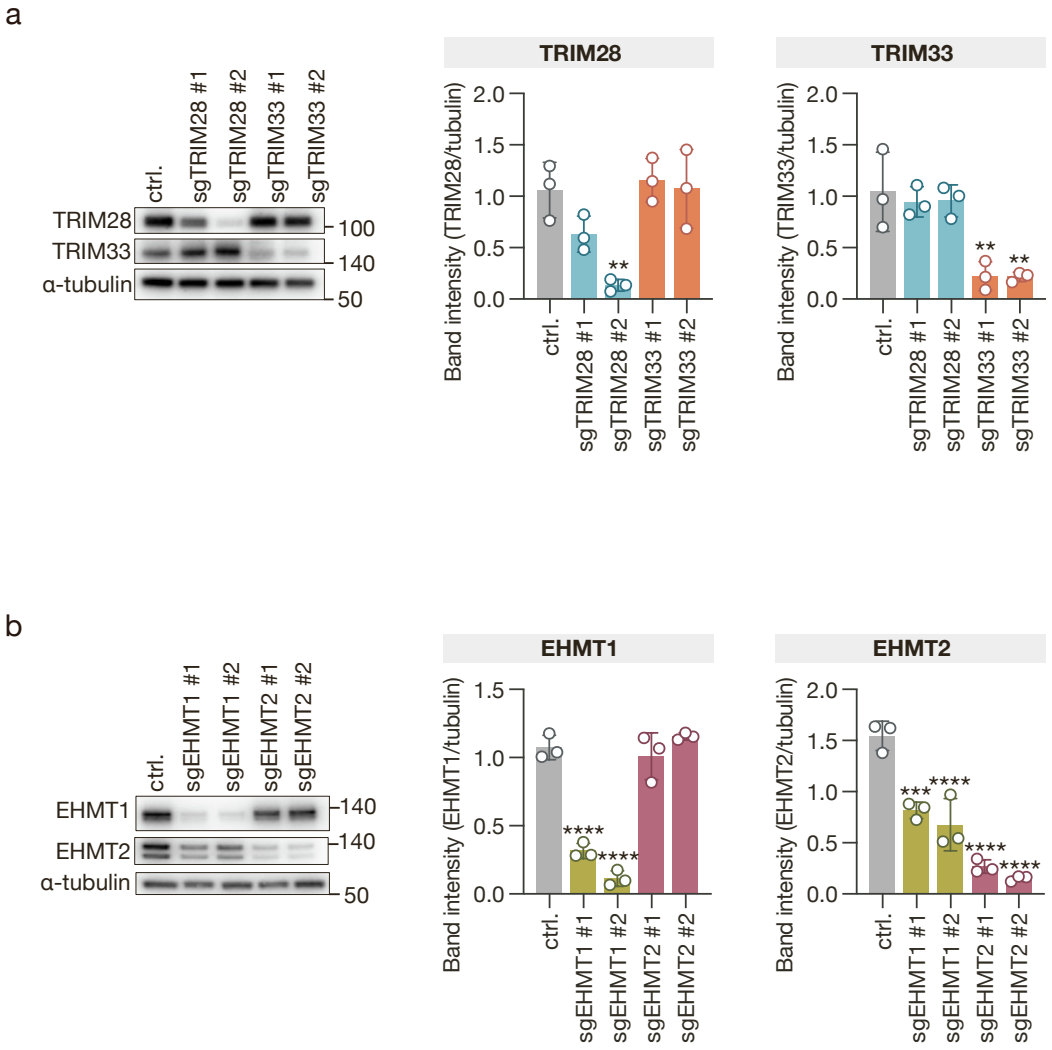

Fig. S3. Knockout efficiency of selected genes in A549-Cas9 cells. Related to Figure 2

(a)(b) Western blotting analysis of selected genes, TRIM28 and TRIM33 (a) and EHMT1 and EHMT2 **(b).** The expression levels were evaluated by the band intensity, which was normalized to that of α-tubulin. Data are presented as the mean ± the SD of three independent experiments. Dunnett's multiple-comparison test. **, $p < 0.01$; ***, $p < 0.001$; **, $p < 0.0001$.

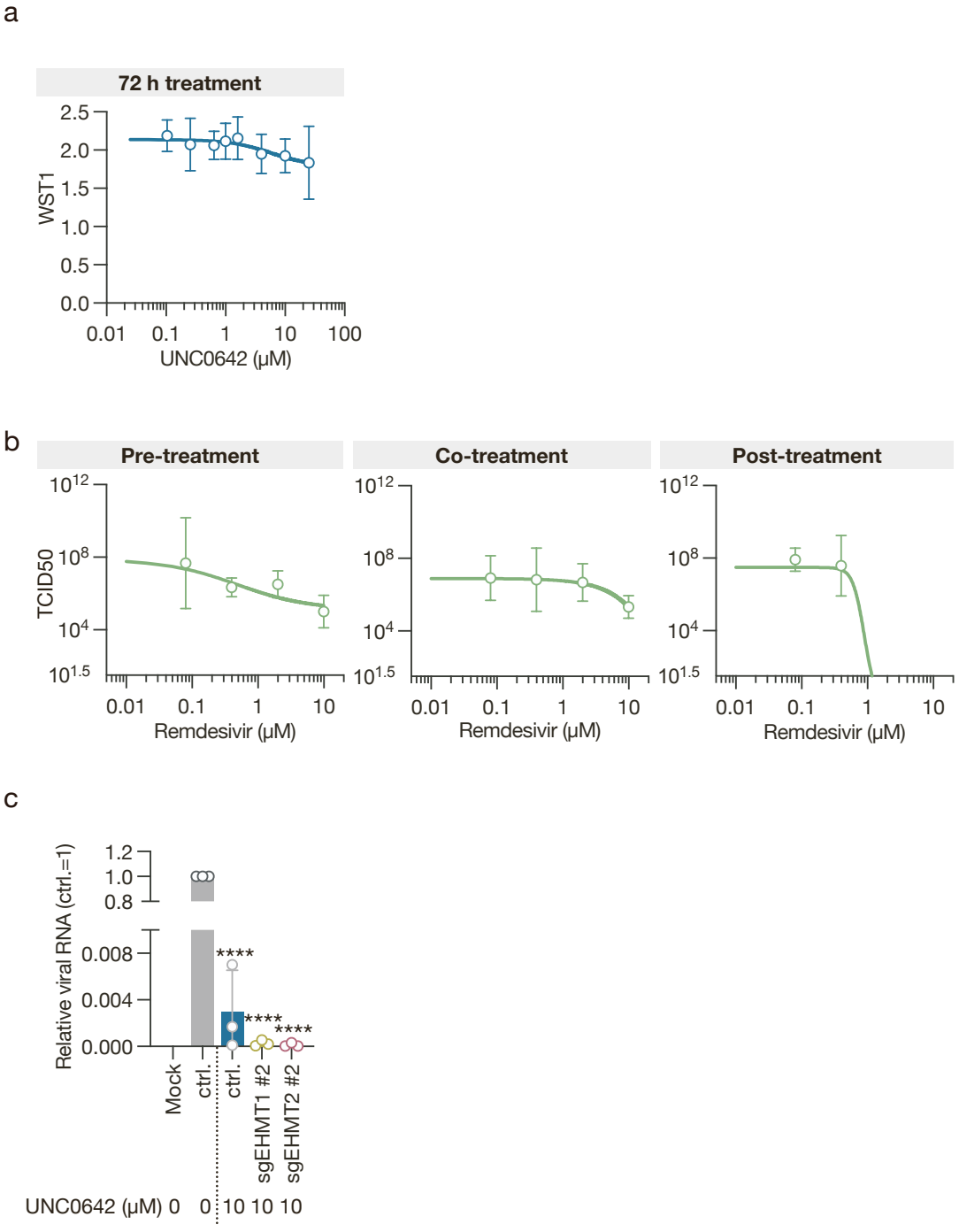

Fig. S4. Evaluation of UNC0642 cytotoxicity and the antiviral effects of remdesivir on SARS-CoV-2. Related to Figure 5

(a) Cytotoxicity of UNC0642 was assessed by monitoring cell proliferation using a WST-1 assay (TaKaRa). This assay measures the cell viability and proliferation, providing insights into the

potential toxic effects of UNC0642 on A549-hACE2 cells. **(b)** The inhibitory effect of remdesivir on SARS-CoV-2 infection was evaluated under different treatment conditions: pre-treatment (1 hour before virus inoculation), co-treatment (during 1 hour virus absorption), and post-treatment (after inoculation). These conditions were designed to assess the effectiveness of remdesivir at various stages of viral infection. Statistical analysis was performed using Dunnett's multiple-comparison test; however, no significant differences were observed under any of the treatment conditions. (c) qPCR analysis of viral RNA in EHMT1, or EHMT2 knockout cells treated post-infection with 10 μM UNC0642 for 3 days. The cells were inoculated at an MOI of. 0.001. Data are presented as the mean ± SD of three independent experiments. Statistical analysis was performed using Dunnett's multiple-comparison test. ****, $p < 0.0001$.

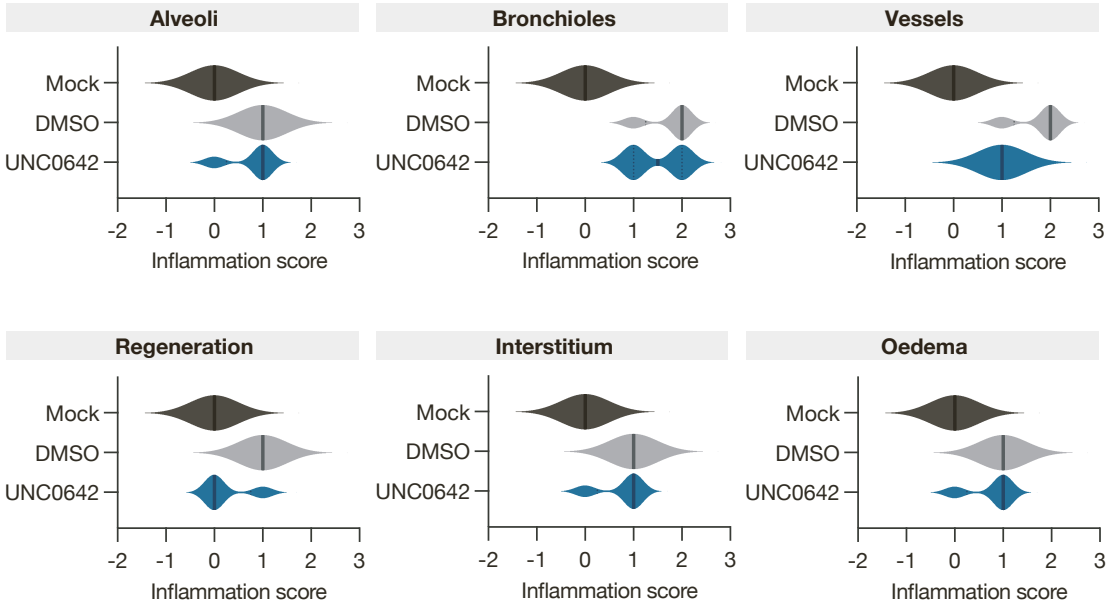

Fig. S5. Pathological scoring of various tissue responses in hamster lungs post SARS-CoV-2 infection. Related to Figure 6

This figure presents a violin plot illustrating the distribution and intensity of inflammation scores in the lungs of hamsters, assessed 4 days post-infection with SARS-CoV-2. The scores encompass a range of pathological features including changes in the airways, interstitial spaces, blood vessels, and alveolar structures, as well as the presence of oedema and signs of alveolar epithelial regeneration.